Oil Shale, 2024, Vol. 41, No. 2, pp. 115–131
doi: https://doi.org/10.3176/oil.2024.2.03
ISSN 0208-189X

Optimization of nozzle structure of top-burning heating furnace: case study of Fushun retort heating for oil shale

Yue Yue[(a,b)*], Zhu He[(a)], Chunhua Wang[(b)*]

[(a)] Department of Materials, Wuhan University of Science and Technology, Wuhan 430065, China
[(b)] College of Petroleum Engineering, Liaoning Petrochemical University, Fushun 113001, China

Received 5 February 2024, accepted 19 April 2024, available online 30 April 2024

Abstract. *The purpose of this study is to introduce an air nozzle on top of a top-fired heating furnace designed for oil shale retorting, using numerical simulations to delineate enhanced gas flow, heat transfer, and combustion in the furnace. Traditional heating flow fields, temperatures, and nitric oxide (NO) emission behaviors were carefully studied alongside furnaces fitted with various top jet systems. Our findings conclude that the introduction of top air supply leads to the development of a stable vortex pair in the combustion chamber, enhancing flame stability. Moreover, the incorporation of the top jet structure noticeably enhances the combustion chamber's temperature and homogeneity, retaining the benefits of swirl combustion, optimizing high-speed entrainment effects, promoting gas flow stratification, and substantially reducing NO production. With the implementation of the top air supply, NO emission is reduced to below 50 mg/Nm³, while peak incomplete combustion heat loss decreases to less than 1%, which successfully helps achieve the goal of improving thermal efficiency, saving energy, and reducing emissions from the heating furnace.*

Keywords: *oil shale retorting, top-fired heating furnace, air nozzle, NO emission.*

1. Introduction

In the process of oil shale retorting to produce oil, a large amount of gas with low calorific value is generated. In order to utilize this gas, a portion of gas is directed to the heating furnace to provide thermal cycle gas for the retorting furnace, while another portion is used as fuel for the heating furnace. A regenerative heating furnace serves as a heating appliance in the oil

* Corresponding authors, yueyue92976@163.com, wangchunhua@lnpu.edu.cn

shale retorting process using heat carriers [1]. Typically, the heating system employs three heating appliances, including two heating furnaces during the combustion phase and one heating furnace during the heating phase, or vice versa; this rotation is carried out on a regular basis [2].

The top-burning heating furnace is used for retorting oil shale [3]. Its structural design mimics that of the top-burning hot blast stove found in iron smelters. This device conveys heat from fuel combustion through hot air, generating high-temperature and high-pressure air exceeding 1273 K for the blast furnace [4, 5]. The burning heating furnace for retorting oil shale increases the heating level of the circulating gas. The combustion chamber is positioned in the upper part, with a circular mixing chamber located on top of it. Both combustion support air and fuel gas enter the respective ring channels, with the gas subsequently passing through each nozzle and injecting into the mixing chamber due to the internal pressure of the nozzle. The fuel gas and air mix in a continuous process, and the resulting gas is released at a specific speed and direction for combustion. The operating characteristics of the furnace, including the placement of burner nozzles in the combustion chamber and the inclination angle distribution, can significantly affect the burner's performance [6–8].

Understanding and mastering the unique attributes of the furnace is crucial for its effective design, operation, maintenance, and repair. Wang et al. [9] proposed incorporating a slanted guide brick within the gas and oxidizing air loop of the furnace to enhance gas vortex distribution and diffusion. This adjusts the gas mixture for a more uniform distribution and stable vortex in the combustion chamber. Peng [10] substantiated, through numerical simulations, that refining the configuration of gas and combustion-supporting air nozzles, and enhancing their quantity and layers can intensify the contact area between air and fuel gas, facilitating thorough mixing and yielding a more potent vortex in the combustion chamber, thereby increasing combustion efficiency and heat exchange impact.

Li [11] evaluated the effect of varying nozzle configurations on the gas velocity field, temperature field, and pressure field in the furnace by altering the number and orientation of gas and air nozzles. Hao et al. [12] used numerical simulation techniques to probe into the impact of the burner nozzle's radial angle on the flow field and combustion behavior. The findings revealed that at a special angle, the reflux area is relatively wide, which makes the CO distribution range narrow. At the same time, the outlet temperature increases significantly, the temperature difference diminishes considerably, the NO concentration decreases, and the flue gas distribution is more uniform. Zhang et al. [13] elucidated that the conventional nozzle design of the furnace induces high-speed swirl in the flue gas, leading to excessive fluid "attachment" in the combustion chamber. This results in nonoptimal temperature distribution and thermal storage, hotter globe surface, accelerated wear of refractory material, enhanced wall heat dissipation, and decreased thermal efficiency.

To counter this, they proposed upgrading the nozzle structure from an equal diameter cylinder neck to a tapered nozzle design with a wider top section and a narrower bottom section to mitigate fluid attachment.

Qi et al. [4] incorporated three gas and air inlet tubes to rectify the disparities in combustion chamber pressure and temperature distribution. Zhang et al. [14] successfully eliminated the "asymmetric swirl" dilemma prevalent in traditional heating furnaces by alternating the gas and air nozzles within the same layer. This strategy bolsters heat transfer efficiency and heat storage capacity, fostering a more uniform and efficient combustion process. Wei et al. [15] employed a catenary vault structure and annular staggered upjet hybrid burner to optimize the distribution of the flue gas flow field, and minimize temperature discrepancies between the vault and supply air temperatures. Additionally, they chose a burner technology with a low air excess coefficient (i.e., annular staggered upjet hybrid burner) for the purpose of reducing NO_x emissions.

The above research focuses on the thermal efficiency, pressure distribution, velocity distribution, and temperature distribution of the top-fired heating furnaces in the steel industry, and there is little research on NO_x emissions from heating furnaces. However, research on top-fired heating furnaces for oil shale retorting is scarce. The modifications made to the basic structure of hot blast furnace nozzles and combustion chambers are a significant contribution that could be applied to oil shale retorting furnaces. The combustion process and efficiency of the furnace have a direct impact on oil shale retorting. For steady and efficient operation, the furnace should supply consistently stable thermal cycle gas to the retorting furnace. Therefore, it is very important to study and analyze the operating characteristics of the heating furnace.

This study used operational data from a shale oil plant's top-fired heating furnace to construct a simplified three-dimensional model of the furnace, using modeling software and simulating its operating conditions. The gas velocity field, temperature field, and NO_x emissions at the furnace's outlet were analyzed under different nozzle arrangements to identify an optimal design improvement for superior operational performance and value, especially in compliance with increasingly stringent NO_x emission regulations.

2. Mathematical models

2.1. Turbulent flow model

The realizable k-ε model, chosen for its aptitude in portraying the jet types of fuel and air inflow in gas and air nozzles, is extensively utilized for turbulent phenomenon representation. This model excels in simulating the generation, transmission, and attenuation of eddy currents, portraying fuel and air jet behaviors in furnaces with high precision. The k and ε transport equations are expressed as follows [16]:

$$\frac{\partial(\rho k u_i)}{\partial x_i} = \frac{\partial}{\partial x_i}\left[\left(\mu + \frac{\mu_t}{\sigma_k}\right) + \frac{\partial k}{\partial x_i}\right] + G_k + G_b - \rho\varepsilon - Y_M, \quad (1)$$

$$\frac{\partial(\rho\varepsilon u_i)}{\partial x_i} = \frac{\partial}{\partial x_i}\left[\left(\mu + \frac{\mu_t}{\sigma_\varepsilon}\right)\frac{\partial \varepsilon}{\partial x_i}\right] + \rho C_1 S\varepsilon - C_2\rho\frac{\varepsilon^2}{k+\sqrt{v\varepsilon}} + C_{1\varepsilon}\frac{\varepsilon}{k}C_{3\varepsilon}G_b, \quad (2)$$

where ∂ is a partial differential notation, ρ is the density, u_i is the average velocity of the fluid in the i direction, k is the turbulent kinetic energy, ε is the turbulent kinetic energy dissipation term, the lower corner mark i indicates the direction of fluid flow, μ is the dynamic viscosity, μ_t is the turbulent viscosity, G_k is the turbulent energy generated by the mean velocity gradient, G_b is the turbulent kinetic energy generated by buoyancy, Y_M is the contribution of wave expansion to the total dissipation rate in compressible turbulence, σ_k and σ_ε are the turbulent Prandtl numbers of k and ε, respectively, and C_1, $C_{1\varepsilon}$, C_2, and $C_{3\varepsilon}$ are constants.

2.2. Combustion model

Fuel and air are not mixed before entering the combustion chamber. Instead, a non-premixed combustion model is used, facilitating comprehensive simulation and understanding of the dynamics of non-premixed combustion. Mathematical expressions are as follows [16]:

$$\frac{\partial\left(\rho\bar{f}\right)}{\partial t} + \frac{\partial\left(\rho u_j \bar{f}\right)}{\partial x_j} = \frac{\partial}{\partial x_j}\left(\frac{\mu_t}{\sigma_t}\frac{\partial \bar{f}}{\partial x_j}\right), \quad (3)$$

$$\frac{\partial}{\partial t}\left(\rho\bar{f}'^2\right) + \frac{\partial}{\partial x_j}\left(\rho u_j \bar{f}'^2\right) = \frac{\partial}{\partial x_j}\left(\frac{\mu_t}{\sigma_t}\frac{\partial \bar{f}'^2}{\partial x_j}\right) + C_g\mu_t\left(\frac{\partial \bar{f}}{\partial x_j}\right) - C_d\rho\frac{\varepsilon}{k}\bar{f}'^2, \quad (4)$$

$$f = \frac{Z_i - Z_{i,ox}}{Z_{i,fuel} - Z_{i,ox}}, \quad (5)$$

$$f' = f - \bar{f}, \quad (6)$$

where t is time, the lower corner mark j indicates the direction of fluid flow, f denotes the mixed fraction, $\bar{f}$ is the mean (time-averaged) mixed fraction, $\bar{f}'$ is the mean mix-fraction variance, σ_t, C_g and C_d are equation constants, which equal to 0.85, 2.86, and 2.0, respectively, Z_i is the elemental mass fraction of some element i, $_{ox}$ is the value of the oxidant inlet, and $_{fuel}$ is the value of the fuel inlet.

2.3. Radiation heat transfer model

The radiation heat transfer model selects the discrete ordinates (DO) radiation model, which can be used to simulate the radiation heat transfer process on the surface of the object and in the fluid medium. This is expressed as follows [16]:

$$\frac{\mathrm{d}I\left((\vec{r},\vec{s})\vec{s}\right)}{\mathrm{d}s}+(\alpha+\sigma_s)I(\vec{r},\vec{s})=an^2\frac{\sigma T^4}{\pi}+\frac{\sigma_s}{4\pi}\int_0^{4\pi}I(\vec{r},\vec{s}')\Phi(\vec{s},\vec{s}')\mathrm{d}\Omega', \tag{7}$$

where d is the derivative sign, T is the temperature, I denotes radiant intensity, $\vec{r}$ is the position vector, $\vec{s}$ is the unit vector in dispersal direction, $\vec{s}'$is the unit vector in incidental radiation path, α is the absorption rate, n is the refraction coefficient, σ is the Stefan-Boltzmann constant, σ_s is the scattering rate, Ω' is the solid angle, and Φ is the phase function.

2.4. NO_x generation model

NO_x derived from gas combustion covers only thermal and rapid NO_x, excluding fuel NO_x. Specifically, the main NO_x component of gas combustion is NO. The rapid NO generation rate is expressed as follows [16]:

$$\frac{\mathrm{d}[NO]}{\mathrm{d}t}=f_c k_{prompt}[O_2]^a[N_2][fuel]\exp\left(\frac{E_a}{RT}\right), \tag{8}$$

$$k_{prompt}=6.4\times10^6\left(\frac{RT}{p}\right)^{a+1}, \tag{9}$$

$$f_c=4.75+0.0819n-23.2\psi+32\psi^2-12.2\psi^3, \tag{10}$$

where d is the derivative sign, t is the time, a denotes the order of O_2's reaction, E_a is the activation energy, R is the universal gas constant, f_c is the correction factor dependent on the fuel category and fuel-air ratio, T is the fluid temperature, Ψ is the equivalent ratio, and p is pressure.

Obtained from Eqs (8) and (9), the reaction order a for O_2 is determined:

$$a=\begin{cases}1.0 & X_{O_2}<4.1\times10^{-3}\\ -3.95-0.9\ln X_{O_2} & 4.1\times10^{-3}\le X_{O_2}<1.11\times10^{-2}\\ -0.35-0.1\ln X_{O_2} & 1.11\times10^{-2}\le X_{O_2}<3\times10^{-2}\\ 0 & 3\times10^{-2}\le X_{O_2}\end{cases}. \tag{11}$$

The thermal NO_x generation rate is expressed as follows [16]:

$$\frac{\mathrm{d}[NO]}{\mathrm{d}t}=22k_1[O][N_2]\frac{\left(1-\frac{k_{-1}k_{-2}[NO]^2}{k_1[N_2]k_2[O_2]}\right)}{\left(1+\frac{k_{-1}[NO]}{k_2[O_2]+k_3[OH]}\right)}, \tag{12}$$

where the reaction coefficients are given as follows: $k_1=1.8\times10^8e^{-38370/T}$; $k_{-1}=3.8\times10^7e^{-425/T}$; $k_2=1.8\times10^4e^{-4680/T}$; $k_{-2}=3.81\times10^3e^{-20820/T}$; $k_3=7.1\times10^7e^{-450/T}$.

3. Research object

A top-burning heating furnace for dry distillation of oil shale adopts an integral cylindrical design, with a semi-arc top covering. It is composed of a burner, a pre-combustion chamber, a combustion chamber, and a regenerator chamber. The operation of the heating furnace comprises two stages: combustion and heating.

As illustrated in Figure 1, during combustion, combustible gas and air are introduced into the pre-combustion chamber via separate pipes for mixing, combusting in the chamber, and generating flue gas in high temperature. This flue gas traverses through the heat storage body in the regenerator chamber, converting it into a high-temperature storage unit. Simultaneously, the cooled flue gas is expelled from the exhaust port at the base of the furnace.

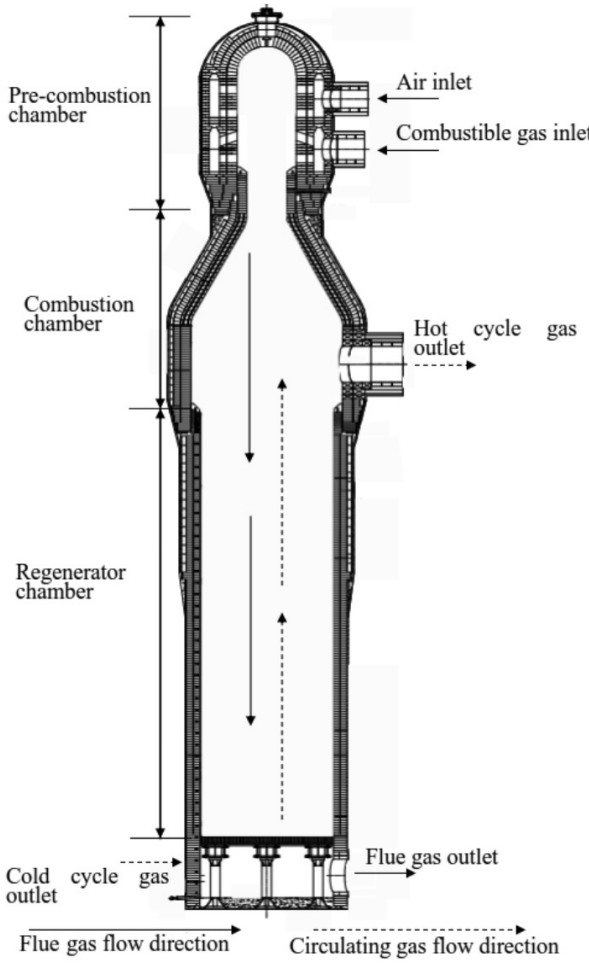

Fig. 1. Structure diagram of top-fired heating furnace.

Once the combustion stage concludes, the heating furnace stops burning, and the reversing valve is reversed to enter the heating stage. When the heating stage commences, cold cycle gas enters the regenerator chamber, absorbing thermal energy from the high-temperature storage body and forming hot cycle gas, which serves as the hot carrier gas for future use in a retort furnace. The furnace operates periodically through combustion and heating stages. Over time, the heat stored in the furnace diminishes, preventing the cold circulating gas from reaching the required temperature. Consequently, the heating stage transitions into the combustion stage. By repeating this cycle, the furnace continuously heats and exchanges calorific energy. Typically, three sets of such furnaces are installed and operated sequentially to achieve either the two-burn, one-feed or two-feed, one-burn cycle mode [21].

NO_x production predominantly occurs in the combustion chamber. To highlight this key point and improve calculation efficiency, this study focuses on the pre-combustion and combustion chambers of the furnace, as shown in Figure 1. The height of the pre-combustion chamber is 6400 mm, with a diameter of 4484 mm. The combustion chamber measures 7247 mm in height and 6640 mm in diameter. The fuel used in the furnace is derived from the exhaust gas generated during the oil shale retorting process, and its composition is outlined in Table 1.

Table 1. Gas composition

Component	CH_4	H_2	C_2H_4	CO	CO_2	N_2
%vol	6.0	11.0	1.0	4.0	20.4	57.6

4. Traditional heating furnace calculation and result analysis

4.1. Grids and boundary conditions

The furnace comprises four layers of nozzles: two upper gas nozzles (12 per layer), staggered with a 0° angle both horizontally and vertically, positioned one above the other. The lower two layers consist of 24 air nozzles each, following the same pattern as the upper layer but with a 0° center line angle for the upper nozzle, 19° vertical inclination, and a 0° angle for the lower layer, as shown in Figure 2.

A mixed mesh covers the entire area, employing a tetrahedral mesh for the pre-combustion chamber due to its intricate gaseous and air nozzle connections, using local encryption. The remainder employs a hexahedral mesh, as shown in Figure 3. Post-independent grid analysis yields a total number of approximately 3 million regional grids.

The fuel and air inlets employ velocity inlets, and the section connecting the combustion and heat storage chambers is regarded as the flue gas outlet, with the boundary set as the pressure outlet. For the specific values, see Table 2.

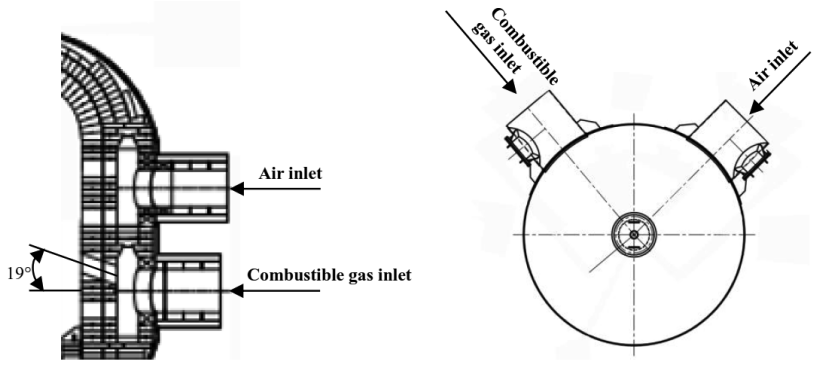

Fig. 2. Structure diagram of air and combustible gas nozzles.

Table 2. Boundary conditions

Fuel inlet			Air inlet		
Velocity, $m \cdot s^{-1}$	Temperature, K	Equivalent diameter, mm	Velocity, $m \cdot s^{-1}$	Temperature, K	Equivalent diameter, mm
8.383	324.15	581	5.905	274.15	693

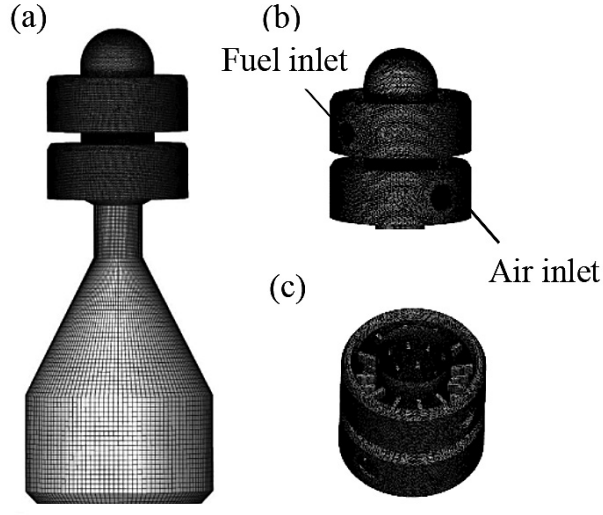

Fig. 3. Grid division: overall calculation area (a), fuel and air nozzles (b), fuel and air flow channels (c).

4.2. Verification of the numerical simulation method

The accuracy of the numerical simulation method was verified by assessing the operating parameters of two identical top-fired heating furnaces, designated as Nos 1 and 2. Test point 1, located at the top of the furnace, 28.19 meters from the base, monitored the temperature of the dome area. Test point 2, located 17.11 meters from the base, measured the temperature of the combustion chamber. Simulations were conducted to analyze the operating conditions of the two furnaces, and the calculated results were compared with the measurements obtained from test points 1 and 2. In addition, NO emission at the furnace outlet was evaluated.

Based on the calculated errors, as shown in Table 3, the simulation-derived predictions closely matched with the measured values, with a maximum discrepancy of only 6.5%. This establishes the reliability of the numerical simulation method employed in this study.

Table 3. Comparison of numerical simulation data and measured data

No.	Data status	Temperature				NO emission value at the furnace outlet	
		Test point 1		Test point 2			
		Value, K	Error, %	Value, K	Error, %	Value, mg/Nm^3	Error, %
1	Measured data	618	6.1	1146	4.6	27	3.7
	Simulation data	656		1199		28	
2	Measured data	621	–5.3	1145	5.1	43	6.5
	Simulation data	588		1203		45.8	

4.3. Analysis of results

In order to compare and analyze different characteristics among cases, the $Z = 0$ plane is selected as a reference, and the streamline distribution, mixture fraction distribution and temperature distribution are studied on this plane, and comparative studies are carried out. Figure 4 illustrates the fluid distribution of the pre-combustion and combustion chambers of the conventional heating furnace, with sections (a) and (b) representing the planes of the secondary layer fuel nozzle and the air nozzle, respectively. As the center line of all nozzles aligns with the cross-sectional radius of the pre-combustion chamber at the nozzle, the respective nozzle jet becomes a countercurrent jet, generating

numerous small vortices on the cross-section. The gas emitted from the gas nozzle enters the hearth. Due to the dilation of the passage, the gas is compressed by the opposing air flow, and a portion of the air flow travels to the dome region, touches the arch wall, and returns, forming a minor reflux area near the dome wall. Another portion flows directly to the outlet of the combustion chamber and meets the rest of the air flow. In the throat, due to the sudden expansion of the combustion chamber, reflux areas are formed on both sides of the combustion chamber, although with slight asymmetry.

Fuel-air mixtures are represented by the mixture fraction, as shown in Figure 5a. When thoroughly combusted, the mixture fraction equates to 0.52, corresponding to an excess air coefficient of 1, thereby yielding a high-temperature flame. Regions with local mixture fractions exceeding 0.52 signify richer fuel areas, while those below 0.52 represent poorer fuel zones. Above the throat, the mixture fraction lies primarily between 0.95 and 1, indicating poor fuel-air mixing in the pre-combustion chamber. This corroborates weak air upflow, leading to diminished pre-combustion chamber temperatures. Beneath the air nozzle, fuel and air gradually intermix, experiencing slow chemical reactions and low combustion temperatures (Fig. 5). As the mixed airflow descends, it encounters the throat segment with a reduced cross-section, resulting in intensified gas-air mixing. Below the throat, the mixture fraction gradually approaches 0.52, initiating proper combustion, and resulting in a vigorous combustion zone and a high-temperature region. Consequently, this leads to a higher NO emission value of 183.41 mg/Nm^3 at the combustion chamber outlet.

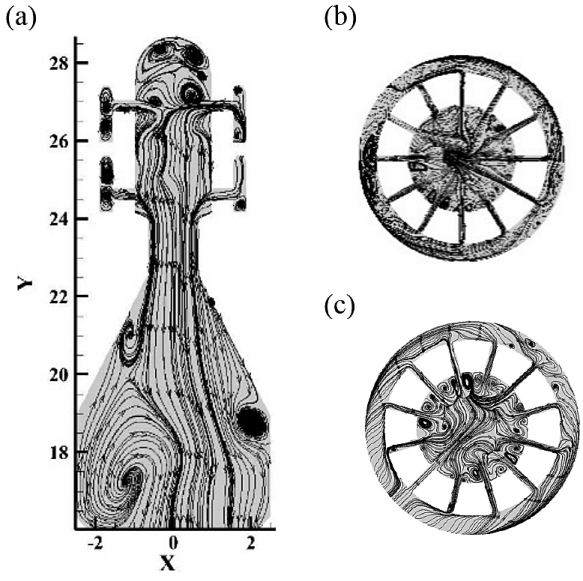

Fig. 4. Velocity streamline in the combustion compartment of the traditional heating furnace: (a) represents the Z = 0 plane, (b) and (c) represent the planes of the secondary layer fuel nozzle and the air nozzle, respectively. X and Y (m) represent the coordinates on the Z = 0 plane.

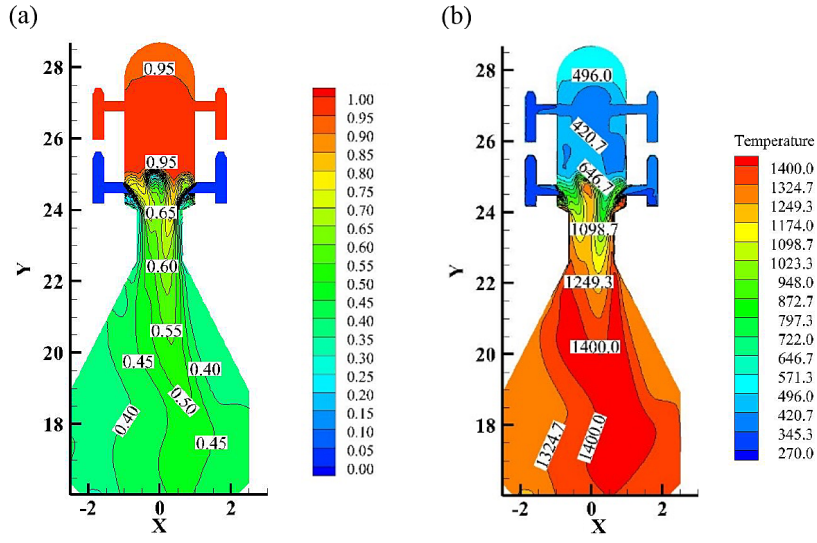

Fig. 5. Mixture fraction distribution (a) and temperature distribution, K (b) in the combustion chamber of the traditional heating furnace (Z = 0 plane). X and Y (m) represent the coordinates on the Z = 0 plane.

Our calculations show a highly asymmetrical distribution in the combustion chamber of the traditional heating furnace, which severely inhibits flame stability. At the same time, there is a marked lack of uniform combustion temperature and elevated NO_x emission values. In light of these findings, optimizing the operating parameters of the heating furnace becomes imperative. This study focuses on the improvement and analysis of the nozzle structure of the heating furnace to achieve flame stability, uniform temperature distribution, and low NO_x emissions.

5. Enhanced heating furnace calculation

5.1. Improved structure

The updated heating furnace nozzle replaces the traditional top-fired furnace design with a configuration that places the air nozzle directly on the furnace top. This aims to expand the range of fuel and air mixing, thus facilitating full air-fuel mixing before entering the combustion chamber.

As illustrated in Figure 6, the fuel gas nozzle is equipped with two layers. The angle between the nozzle central line and the horizontal radial angle measures 30°, the vertical elevation angle equates to 0°, and the two layers of nozzles are arranged intersectively, with 12 nozzles per layer, yielding a total

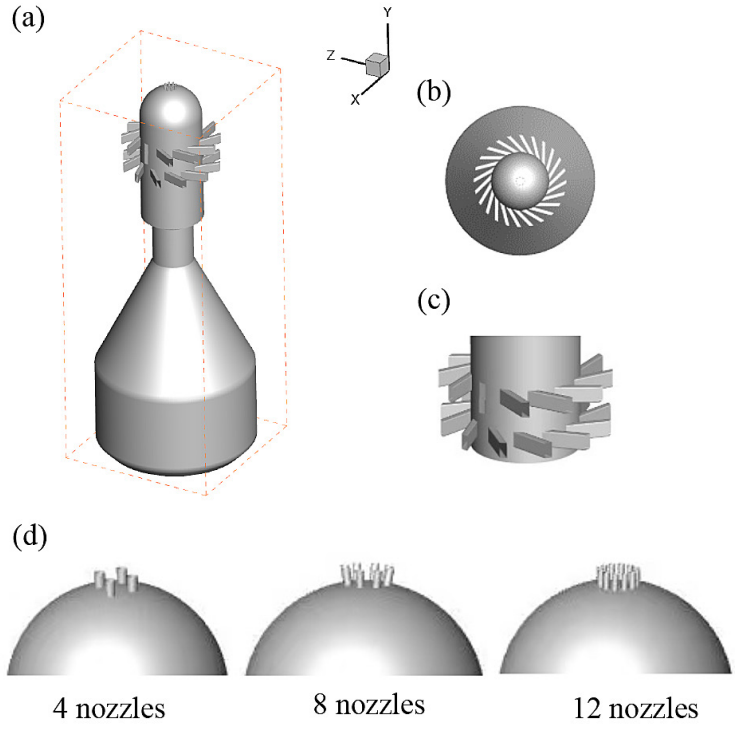

Fig. 6. Structural layout of the furnace body after improvement: main body of the heating furnace calculation area (a), top view of the fuel gas nozzle (b), front view of the fuel gas nozzle (c), arrangement diagram of the air nozzles (d).

of 24 nozzles. The air nozzle is positioned at the apex. To assess the benefits of the top air supply, four distinct air nozzles (1, 4, 8, 12) are considered, along with three diverse air nozzles and the axis inclination (0°, 5°, 10°) for investigation.

5.2. Analysis of results

As shown in Figure 7, distinct symmetrical vortices are discernible at the lower section of the fuel nozzle and on both sides of the combustion chamber after all primary air exits from the top. The fuel rotates in the pre-combustion chamber, leading to visible layered flow patterns: the upper airflow propels due to the suction effect of the top high-speed air flow, completely filling the top region and merging with the departing air from the top nozzle; the lower airflow descends and experiences high-speed impact, forming a rotary vortex. The ejection of primary air accelerates fuel movement along the path, triggering upward diffusion; the descent of the lower fuel flow results in an obvious fuel stratification effect.

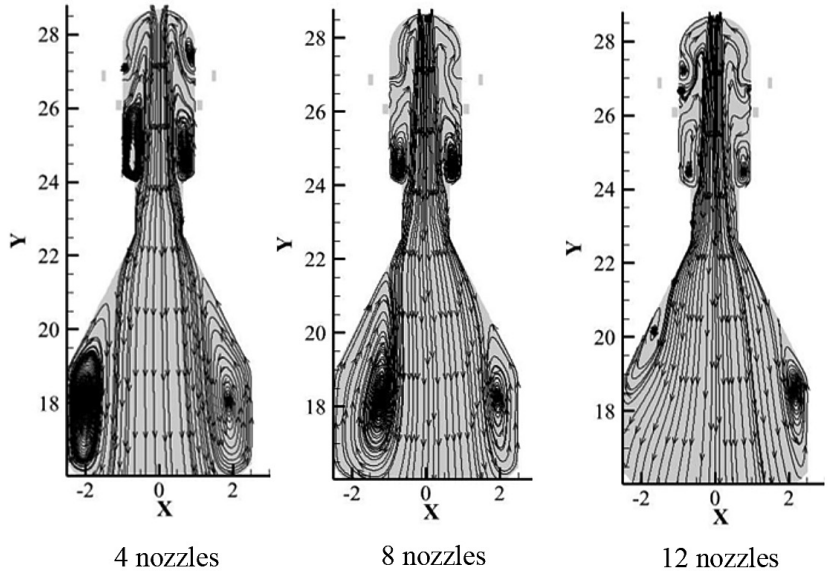

Fig. 7. Streamline distribution in the combustion chamber of the improved heating furnace (Z = 0 plane). X and Y (m) represent the coordinates on the Z = 0 plane.

This expanded space and duration for fuel-air mixing, as shown in Figure 8, results in superior mixing processes in the pre-combustion chamber. However, when the number of nozzles is 12, the stability and symmetry of the vortex generation are slightly inferior compared with the previous two conditions. The increase in the number of top airflow strands significantly changes the vortex size of the preheating furnace, with the vortex diameter gradually decreasing. Assuming equal airflow conditions, an increase in nozzle count and strand number leads to rapid airflow depletion and attenuates the gas flow blocking effect, significantly reducing the vortex diameter. In general, the gas-air and mixing flow fields in the top air supply mode considerably outperform traditional air supply modes.

As shown in Figure 9, after the fuel gas swirls into the interior space of the heating furnace, a portion of the gas rises towards the dome area and intersects with the air expelled from the top nozzles, enabling diffusion combustion, thereby generating localized elevated temperature in a confined area. As the top air jet stream continues to flow downward, the mixing of air and gas gradually becomes substantial, and the chemical reaction continues to intensify, culminating in an elevated temperature of 1400 K at the bottom of the pre-combustion chamber and throat. Compared with the conventional top-fired heating furnace, the chemical reaction between gas and air is more intense, the high temperature zone is established earlier, and the symmetry and uniformity of the temperature distribution exceed those achieved by the traditional heating furnace.

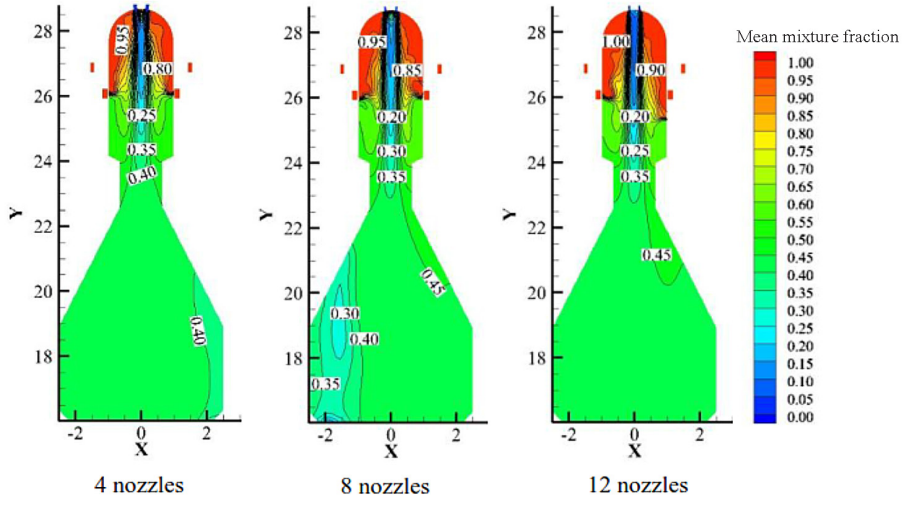

Fig. 8. Mixture fraction distribution in the combustion chamber of the improved heating furnace (Z = 0 plane). X and Y (m) represent the coordinates on the Z = 0 plane.

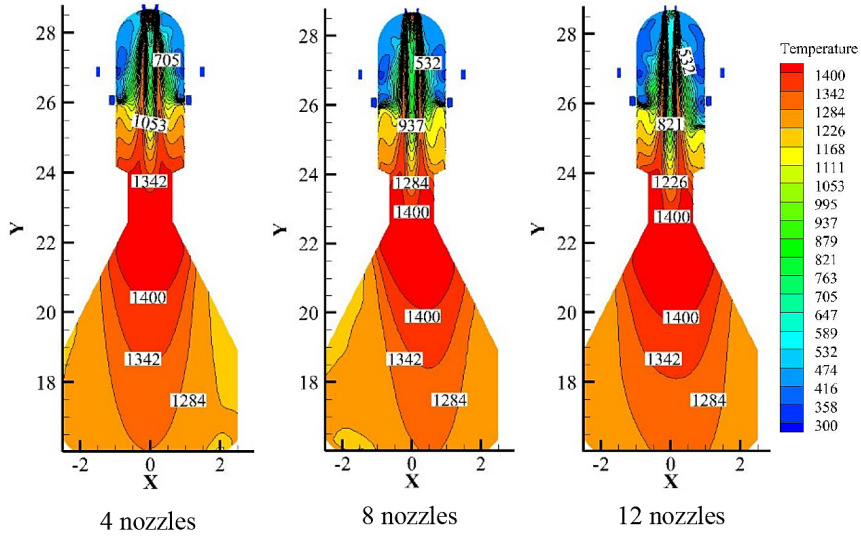

Fig. 9. Temperature distribution (K) in the combustion chamber of the improved heating furnace (Z = 0 plane). X and Y (m) represent the coordinates on the Z = 0 plane.

The implementation of the top air supply increases the average furnace temperature and reduces heat loss from incomplete combustion to below 1%, as shown in Table 4. To evaluate furnace uniformity, a coefficient of heterogeneity is proposed to contrast the distribution of temperature before

and after the improvement. Equation (13) presents the formula for calculating this coefficient [17]:

$$x = \frac{\sqrt{\frac{1}{m}\sum_{j=1}^{m}(T_{lj} - \bar{T})^2}}{\bar{T}}, \tag{13}$$

where T_{lj} refers to point j's temperature in the combustion chamber under a certain case, T is the average chamber temperature, and x is the temperature heterogeneity ratio, with lower ratios suggesting greater uniformity.

The higher the coefficient of heterogeneity, the more uneven the temperature field. The calculations in Table 4 show that the top air supply enhances temperature uniformity in the furnace. At the same time, the level of NO emission flushing out the combustion chamber is substantially lower than the emission level under the traditional air supply technique. All three operating parameters are below 50 mg/Nm^3. Overall, the top air supply increases furnace temperature, reduces heat loss from incomplete combustion, enhances temperature uniformity, reduces NO emissions at the outlet of the combustion chamber, and improves the thermal efficiency of the heating furnace.

Table 4. Comparison of key performance parameters under each case

Case	Traditional furnace	Improved furnace		
		4 nozzles	8 nozzles	12 nozzles
Heterogeneity ratio	0.55	0.38	0.40	0.43
Average temperature, K	1158	1220	1219	1227
NO emission, mg/Nm^3	183.41	40.33	22.10	37.54
Heat loss of incomplete combustion, %	1.3	0.8	0.7	0.5

6. Conclusions

A novel top-fired heating furnace with air nozzles at its apex has been developed for oil shale retorting. Computational fluid dynamics was employed to establish a comprehensive dynamic model of fluid flow, heat transfer, and combustion behavior in the furnace. Analysis of a conventional top-fired hot blast stove and three variants incorporating top jet structures revealed the following:

1. An asymmetrical vortex prevalent in the combustion chamber of the traditional heater destabilized the flame. Switching to the top air supply led to the development of a stable vortex pair, thereby enhancing the stability of the combustion chamber.

2. The introduction of the top jet structure substantially increased the temperature and uniformity of the combustion chamber. With the advantage of retained swirling combustion, high-velocity air entrainment generated a well-graded gas flow, reducing NO production.

3. All three variants using the top air supply exhibited NO emissions below 50mg/Nm^3, incomplete combustion heat loss below 1%, and a significant enhancement in the furnace's thermal efficiency, thus achieving energy conservation and emission reduction objectives.

Acknowledgments

This work was financially supported by the Scientific Research Project of the Education Department of Liaoning Province (No. L2020028). The publication costs of this article were partially covered by the Estonian Academy of Sciences.

REFERENCES

1. Liu, G., Sun, P., Ji, Y., Wan, Y., Wang, H., You, X. Current status and energy analysis of oil shale's retorting process in the world. *Petroleum Chemistry*, 2021, **61**(2), 123–138.
2. Ma, G. *Effects of Fushun oil shale retorting operation factors optimization*. MD thesis. Jilin University, China, 2012.
3. Xu, H., Zhao, Z., Bi, Z. Research on heating furnace technology of Fushun dry distillation technology. *Heilongjiang Science and Technology Information*, 2017, **1**(40), 40.
4. Qi, F., Liu, Z., Yao, C., Li, B. Numerical study and structural optimization of a top combustion hot blast stove. *Advances in Mechanical Engineering*, 2015, **7**(2), 709675. https://doi.org/10.1155/2014/709675
5. Gan, Y. F., Jang, J. Y., Wu, T. Y. 3D dynamic thermal and thermomechanical stress analysis of a hot blast stove. *Ironmaking & Steelmaking*, 2020, **47**(9), 959–972.
6. Zhao, M., Pan, Y., Meng, F., Ma, P., Jia, L., Ma, G., Meng, F., Li, D. CFD numerical simulation of operation optimization for energy saving during combustion period of Kalugin top combustion hot blast stove. *Transactions of the Indian Institute of Metals*, 2023, **76**(7), 1967–1976. https://doi.org/10.1007/s12666-023-02903-7
7. Dai, F. Q., Huang, S. Y., Li, S. H., Liu, K. Study of a ceramic burner for shaftless stoves. *International journal of minerals, metallurgy and materials*, 2009, **16**(2), 149–153.
8. Guo, H., Yan, B., Zhang, J., Liu, F., Pei, Y. Optimization of the number of burner nozzles in a hot blast stove by the way of simulation. *JOM*, 2014, **66**(7), 1241–1252.

9. Wang, B., Huang, S., Dai, F. Numerical simulations in ceramic burner model of top-firing hot-blast stove. *Energy for Metallurgical Industry*, 2007, **26**(2), 24–27.
10. Peng, C. *Numerical simulation of burners in Karugin top burning hot blast stove*. MD thesis. Chongqing University, China, 2010.
11. Li, Y. *Optimum Design of gas and combustion air nozzle structure of top-combustion hot air stove*. MD thesis. Northeastern University, China, 2017.
12. Hao, X., Zhang, Z., Zhang, S., Bo, F. Research on combustion characteristics of top combustion hot blast stove by radial angle of nozzle. *Industrial Heating*, 2018, **47**(1), 8–11, 16.
13. Zhang, Q., Chen, L., Zhao, C. Numerical simulation of combustion and air supply process and optimal design of traditional top combustion hot blast stoves. *Steel Research International*, 2020, **92**(2). https://doi.org/10.1002/srin.202000311
14. Zhang, Q., Chen, L., Ma, X., Zhao, C. Numerical study of combustion and air supply characteristics and structural optimization of top combustion hot blast stoves. *ISIJ International*, 2021, **61**(1), 62–70.
15. Wei, Q., Ge, L., Liu, S., Fu, Z., Liu, L. Technical points of high air temperature and low nitrogen oxide emission in hot blast stove. *Ironmaking*, 2021, **40**(3), 46–49.
16. ANSYS, Inc. ANSYS FLUENT Theory Guide. Release 2023 R2, Canonsburg, 2023.
17. Tian, L. *Research and optimization of temperature uniformity and process parameters of roller kiln*. MD thesis. Guangdong University of Technology, China, 2020.